



# The Detection of Transient Optical Events at Narrowband Visible Wavelengths

Peter F. Bythrow and Douglas A. Oursler

**R**emote sensing of optical transients represents a paradigmatic shift in approach to the detection and identification of anthropogenic terrestrial events. For the most part, short-lived optical events lasting from tens of milliseconds to a few seconds are either undetectable or ignored by most current satellite remote sensing systems. The work described in this article shows that by disregarding transient data, important information about the event source is discarded. This oversight is significant, since the desired information regarding the source may be gleaned within seconds of event onset. These data give an observer the opportunity to rapidly evaluate and respond. Work to date has focused on high-speed, high-resolution imaging at narrowband visible wavelengths that simultaneously captures transient histories and suppresses background clutter from reflected sunlight. Experiments conducted at Cape Canaveral, Florida, have used a high-speed digital camera system and a narrow band-pass filter centered at 589 nm. These experiments have resulted in characterization of the ignition flash and initial plume signature from several large rocket boosters while suppressing daylight background clutter. (Keywords: Fraunhofer filter, Optical transients, Remote sensing.)

## INTRODUCTION

As viewed from space, the Earth's surface is dotted by short-lived optical emission events. These events range in intensity and duration from modest anthropogenic events such as rocket launches and the detonation of high explosives to intense natural events such as lightning strokes or the occasional meteoric high-altitude explosion. With the notable exception of two NASA space sensors, Optical Transient Detector and Lightning Imaging Sensor (both designed for lightning detection), and one Department of Defense sensor, the Earth remote sensing community has generally overlooked optical events lasting from tens of

milliseconds to a few seconds. Because of sensor or mission design, those events are either undetectable or ignored by most current satellite remote sensing systems.

As a result of discounting or overlooking transient data, a wealth of information about an event is also discarded. Most man-made systems operating in a steady state exhibit start-up transients characteristic of that system. Therefore, analysis of a transient recorded during initialization can reveal specific characteristics of the observed event. The desired information regarding the source can be gleaned from a transient within

seconds of event onset and may provide an observer with the potential for rapid response.

We have focused our efforts in transient detection on the visible portion of the spectrum between  $\approx 400$  and  $900$  nm for four reasons. First, many signals of interest are robust at visible wavelengths. Second, the low background afforded by night and by solar absorption lines in daylight reduces clutter. Third, atmospheric transmission is high, and forward scattering of light in water droplets through a multiple scattering process is preferentially skewed toward the visible. Finally, advanced imaging technology of visible wavelength devices such as large-format, high-speed, frame-transfer focal plane arrays is readily available and is rapidly improving owing to the development of the commercial imaging market.

Our work to date has focused on conducting proof-of-concept experiments with a commercially available high-speed, high-resolution imaging system operating at narrowband sodium (Na) wavelength to simultaneously capture transient histories and to suppress background clutter from reflected sunlight. We have conducted three experiments of this type on three different rocket boosters launched from Cape Canaveral, Florida. A fourth experiment is planned with the cooperation of the Naval Surface Weapons Center at Indian Head, Virginia. These experiments used a high-speed digital camera system and an interference filter centered at 589 nm. They have successfully characterized the ignition flash and initial plume signature from the boosters while suppressing background clutter. These data provide the necessary inputs to models that predict the signature expected from an overhead sensor platform.

## DAY/NIGHT DETECTION

As shown in Fig. 1 (top), the Earth's surface when viewed from space at night in the visible and near-infrared portion of the spectrum is more than 6 orders of magnitude dimmer than when seen at wavelengths longer than about  $3\text{ }\mu\text{m}$ . Simply put, at night it's dark! Thus, from a signal-to-background consideration alone, the advantage of looking at visible wavelengths at night for high-temperature optical transients is obvious. In this case, the clutter does not come from the entire Earth's surface but from lightning, meteors, volcanoes, clouds, and man-made sources.

As opposed to darkness, one of the major stumbling blocks to using visible wavelength detectors when viewing a sunlit scene is the tremendous background signal that must be overcome. This fundamental signal-to-background issue may be addressed in several ways, the simplest of which is to reduce the background in a given pixel. For example, in daylight for

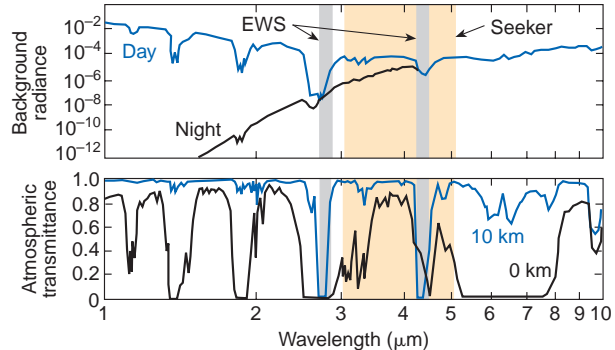


**Figure 1.** Earth's day and night background radiance as seen from space (top) and atmospheric transmittance as seen from altitudes of 10 and 0 km (bottom). Absorption bands due to various atmospheric constituents are seen as lowered transmittance. Bands marked as EWS (early warning system) and Seeker refer to the wavelengths currently considered for missile early warning sensors and seekers.

a conservative background albedo of  $\approx 0.9$ , a broadband point source radiating  $120\text{ kW}$  in a  $10\text{-m}^2$  pixel has a background of  $\approx 12\text{ kW}$ . Therefore, with a  $10\text{-m}^2$  pixel the signal-to-background ratio is about 10. Conversely, if the source remains constant but the pixel includes, for example,  $100\text{ m}^2$ , then the background signal in one pixel is increased by the area ratio to  $\approx 120\text{ kW}$  and the signal-to-background ratio is reduced to 1. If an imager had a ground sample distance of a few meters, the signal-to-background ratio for  $120\text{-kW}$  targets would not be an issue.

For wide-area coverage at high framing rates, this degree of resolution is not practical. Fortunately, another means of addressing the issue is available through narrowband optical filtering. In general, this technique is most effective when the source signal emits in the desired narrow wavelength band and the background does not. For the visible portion of the spectrum, nature provides a set of narrow wavelength absorption bands at which the solar emission is drastically reduced. These absorption lines are called Fraunhofer lines, at which blackbody solar emission is reduced by over 90%. They are the result of the presence of specific elements in the solar atmosphere.

The alkali metals such as sodium or potassium, with their univalent free electron in the outer shell, notably produce very deep absorption features. Figure 2 shows the depth of absorption at various Fraunhofer wavelengths near 600 nm. The Na absorption line exhibits a signal reduction of  $>98\%$  with a line width of  $>0.05\text{ nm}$ . Therefore, the use of a Na transmission filter with a narrow bandwidth should dramatically reduce the overall solar background while retaining the Na signal from the source.

Since clouds of varying thickness often cover the Earth's surface, cloud penetration by light of a specific wavelength is another consideration in the use of the

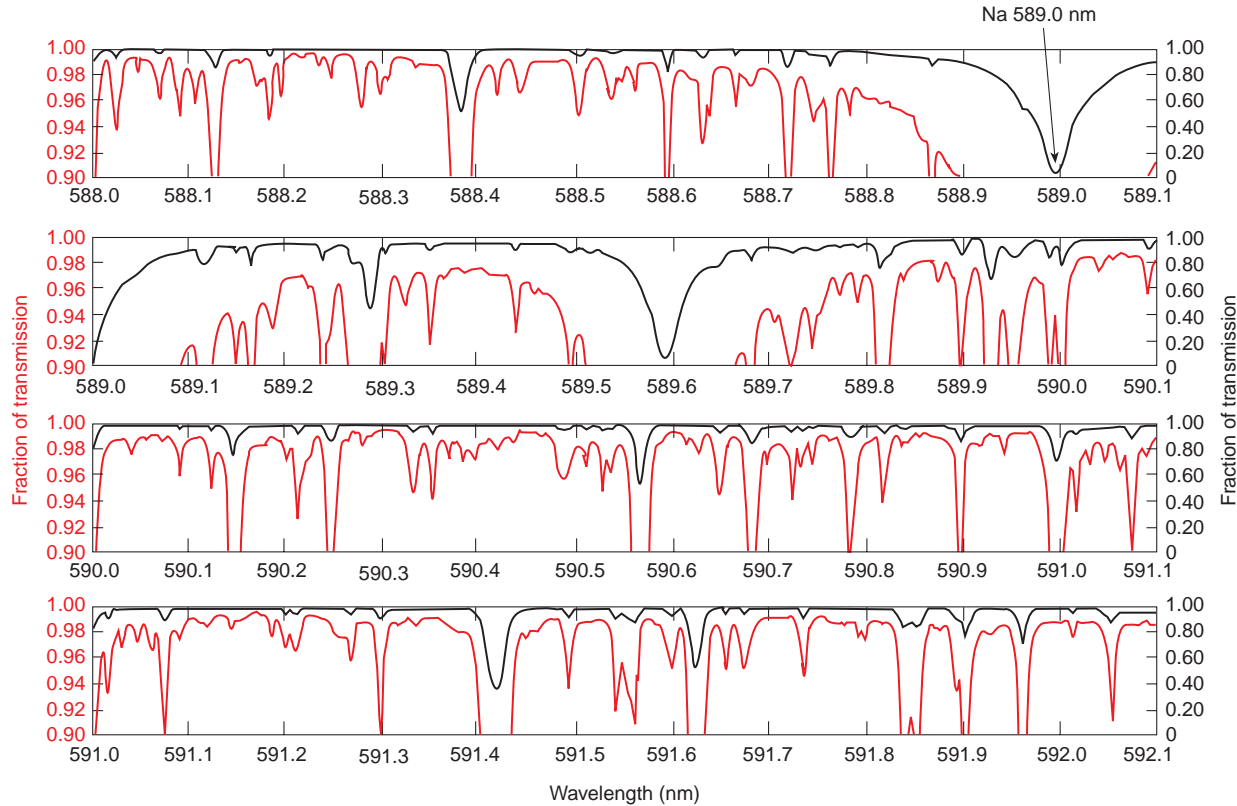


**Figure 2.** Absorption features of the solar spectrum near 600 nm show Fraunhofer absorption lines, in particular, the Na line at 589.6 nm with >98% absorption.

visible spectrum for detection of ground-level optical transients. The scattering of light by water aerosol particles is a function of wavelength and particle size. For particle sizes much smaller than the wavelength ( $\lambda$ ) of the source emissions such as air molecules, Rayleigh scattering dominates the process and the scattering angle is proportional to  $\lambda^4$ . Thus, longer wavelengths are least scattered. However, for particle sizes on the order of, or greater than, the wavelength of the source of illumination, Mie scattering dominates the process. For water droplets of typical size in clouds, wavelengths in the visible spectrum are therefore preferentially forward scattered over longer wavelengths. Multiple scattering interactions with several particles increase the probability of visible-wavelength penetration of clouds and atmospheric water vapor. Hence, a significant portion of the source intensity may penetrate through a cloud layer while retaining information on time history and event location, thereby allowing an optical transient occurring below a cloud layer to be detected from overhead. The clouds, in effect, act as a diffuse back-illuminated projection screen.

Recent experiments conducted by the Air Force Research Laboratory at Hanscom Air Force Base, Bedford, Massachusetts, have detected Na line emissions through overcast clouds. Low-pressure Na lamps,

with a total power emitted on the order of 100 W, were used for these experiments. Measurements were made from an aircraft using an atomic line filter and a photomultiplier tube detector.

## GROUND-BASED INSTRUMENTATION

The development of the concept of optical transient detection by means of a narrowband visible imaging system requires that both the sources of emission and the background be characterized at the specific wavelength selected for observation. For reasons discussed earlier, our efforts have focused on the 588.9973-nm line of Na. We have therefore acquired a Daystar temperature-controlled interference filter centered at that wavelength. The APL Research and Technology Development Center conducted characterization of the filter with a dye laser. The complete instrumentation consists of the filter mated to a 7-in. Maksutov telescope manufactured by Meade Corporation and a high-speed digital camera.

As shown in Fig. 3a, the camera and filter are attached to the telescope via a beamsplitter. A broadband visible camera is attached to the other axis of the beamsplitter to aim and focus the telescope. In

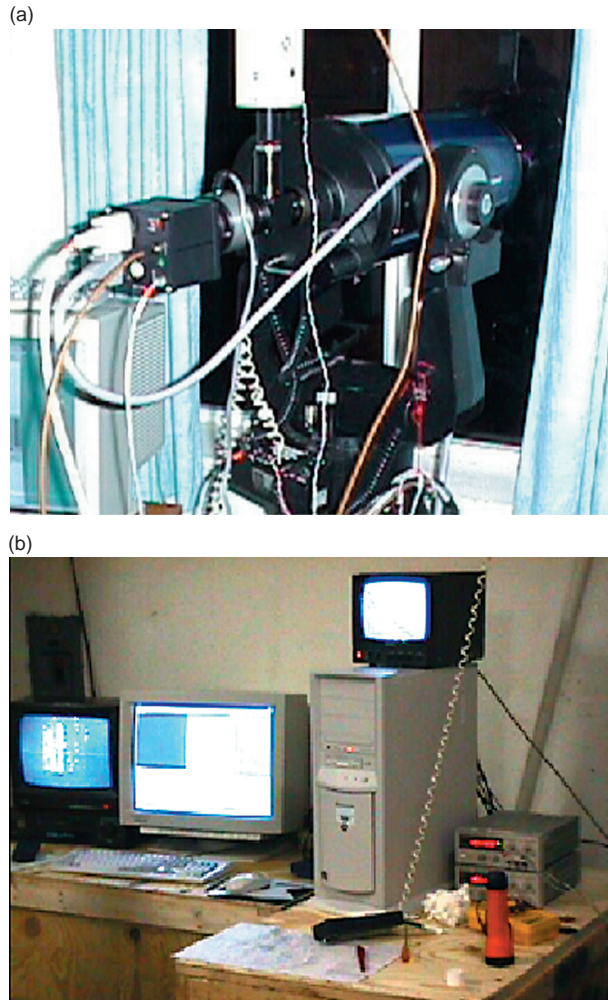


**Figure 3.** Ground-based instrumentation. (a) Setup showing telescope, beamsplitter, Daystar Na filter, and SMD digital camera. The visible color camera is mounted at right angles to the telescope. (b) Computer and monitor setup as configured for the launch of a Titan IV at Cape Canaveral.

addition, this configuration allows us to record the event in the broadband visible spectrum. A low-pressure Na lamp is used to adjust the optical path length of the visible camera to match that of the filtered camera. Therefore, objects in focus at the visible camera are also in focus at the filtered camera. The computer shown in Fig. 3b controls the digital camera. Data from the filtered camera are collected, stored in the computer's memory, and transferred to the hard drive. Broadband data are captured on tape. The system has recently been upgraded, and another digital camera with a cooled focal plane to reduce the detector noise level has been added. The current digital camera will replace the broadband visible camera and allow a direct comparison between broadband and narrowband results. In addition, we have converted a laboratory spectrometer for field use and will include spectral measurements in future observations.

## OBSERVATIONS/MEASUREMENTS

The optical transients produced by rocket boosters and their detection from space are of significant interest to several government agencies. Hence, we selected three different large rocket boosters as candidates for data-collection experiments. For an exceptionally large solid booster, we chose the launch of a Titan IV (T IV) rocket on 12 August 1998. The T IV has roughly 3.4 million pounds of thrust from its solid strap-on boosters. Although the vehicle exploded less than a minute into flight, our data collection was a success. (The central core hypergolic engine of the T IV is not ignited until well into flight. Therefore, launch signatures are entirely from the solid engines.) For a large medium-class solid booster, we chose the inaugural launch of the Delta III rocket on 26 August 1998. Although this booster has a central core fueled with rocket propellant-1 (RP-1), most of the initial  $\approx 800,000$  lb of thrust is from the solid strap-on boosters. Our third experiment was the observation of the all-liquid Atlas 2A rocket with  $\approx 460,000$  lb of thrust fueled with RP-1 and liquid oxygen. Observation of the T IV was made from a range of 11 nmi, whereas for the Delta III and Atlas 2A rockets the ranges were 4 and 6 nmi, respectively. Figure 4 shows the Delta III launch pad from the experimental observation site at Cape Canaveral. The flame ducts that direct much of the energy away from this site extend away from the pad, and beach foliage obscures the very base of the pad.

Daylight observations of the launch pad and booster were made through the Na filter. These data were compared with those taken when the telescope aperture cover was in place, and no discernible difference was detected between the Na background and no



**Figure 4.** A view of the Delta launch pads from the experimental observation site at Cape Canaveral. The Delta III is on the right launch pad.

aperture illumination. Therefore, this sets an upper bound for the background signal level at equal or less than the instrument thermal and read offset levels.

The Delta III launch occurred in darkness at  $\approx 2130$  EST on 26 August 1998. High-resolution imaging data were collected at 7.5 frames per second for the first 8 s of boost. Figure 5 is an excerpt from these data showing six panels in both the narrowband (589 nm) and broadband. In each panel, the development of the plume is separated by approximately 0.5 s. The first three panels show the booster ignition sequence and plume development before the booster left the pad. From our horizontal vantage point, smoke obscuration of the plume is obvious. The data showed a bright, optically thick, resolved plume at the Na wavelength. The intensity increased with time from ignition and then decreased as the plume left the imager's field of view. Despite the smoke obscuration, the measured peak scene intensity projected from a conical Lambertian surface was roughly 3 kW at 589 nm. The plume length, radius, and cone angle were calculated from the observations, as was the booster acceleration. From these data the total plume surface area was determined as  $\approx 850$  m $^2$ , resulting in an average plume intensity of  $\approx 30$  W/m $^2$ .

Another launch observation of some significance was that of the Atlas 2A from pad 36 at Cape Canaveral on 21 October 1998. The plume from Atlas 2A is shown in Fig. 6 in both broadband and narrowband emissions. Unlike the T IV and the Delta III, the Atlas 2A has no solid motors. Its three engines produce  $\approx 460,000$  lb of thrust, and it is fueled with RP-1 (kerosene), with liquid oxygen as the oxidizer.

The key data collected in each of these launch observations are the intensity versus time profiles. These data contribute to what would be detected as an optical transient from a space or airborne sensor platform. Figure 7 shows that the observed intensities scale somewhat as thrust for the solid boosters. The T IV has roughly 4 times the thrust as the Delta III and is roughly 4 times as bright. The Atlas 2A has about half as much thrust as the Delta III, yet is nearly as bright at 589 nm. We are examining reasons for these behaviors and suspect that they may be attributed to a difference in fuel, contaminants, and oxidizer. Finally, each booster has a significant difference in intensity versus time profile that may be attributed to the difference in thrust-to-weight ratios.

## MODEL PREDICTIONS

When observed from overhead, such as from an Earth-orbiting spacecraft, the intrinsic brightness of optical transients produced by rocket boosters appears significantly amplified over the integrated plume

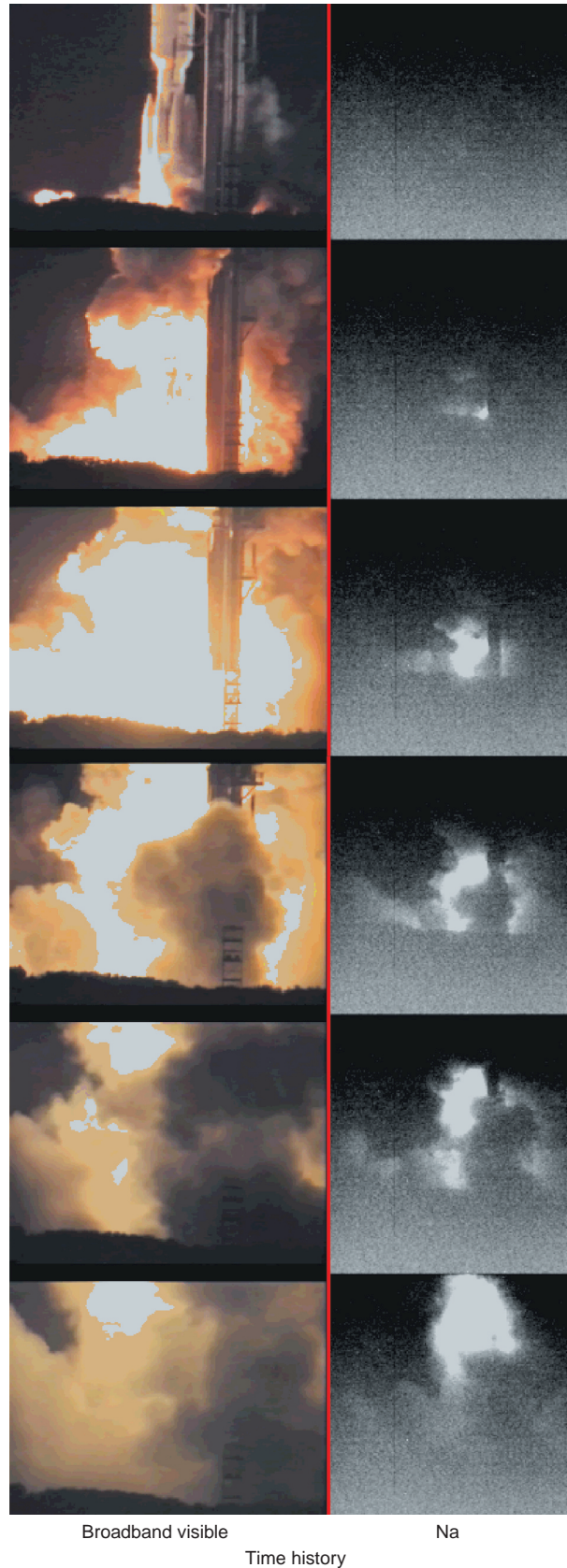


**Figure 5.** Launch sequence of the Delta III booster from Cape Canaveral on 26 August 1998, showing both broadband and Na emissions at 589 nm.

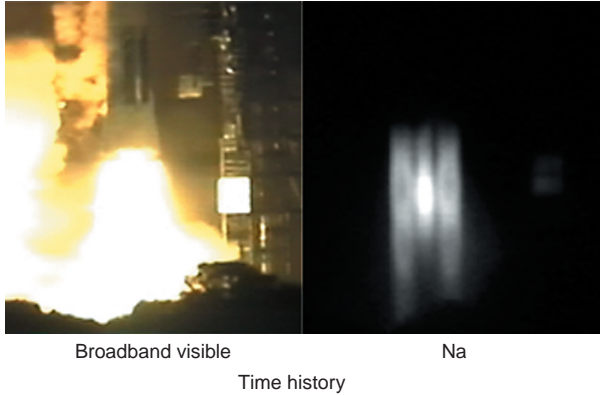


**Figure 6.** Launch of the Atlas 2A on 21 October 1998 showing both broadband emissions on the left and Na emissions on the right at 589 nm. It is significant that the Atlas 2A is fueled with RP-1 and liquid oxygen.

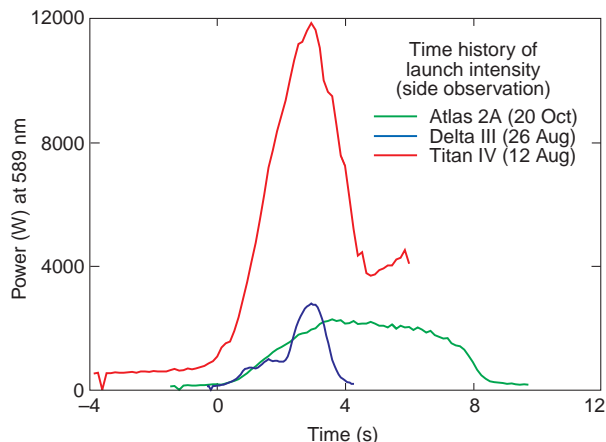


**Figure 7.** Time history profiles (1998) of intensity in watts at 589 nm for each of the three boosters observed. Note that the peak intensity of the Atlas 2A is near that of the Delta III; however, its temporal variation is quite different.

emissions as viewed from right angles. This effect is predominantly seen during the period when the rocket's plume is interacting with the ground.

We have applied a simple geometric model to the measured data from our three booster observations to yield the signal expected when viewed from overhead. In this model, the plume is assumed to remain optically thick and its surface irradiance to remain constant while it is within a few plume lengths of the ground. The model we use is the three-stage process depicted in Fig. 8. Stage 1 assumes a plume irradiance  $I_p$  and an expansion velocity  $V_s$ . The plume expands radially at a velocity  $V_s$  from  $r_{\min}$ , the minimum plume radius, until it reaches a radial distance  $r_{\max}$  roughly equal to the length of the plume  $L_p$ , where  $\rho V_s^2 = P_a$ , the compressed atmospheric pressure. From overhead, the launch flash is a result of a rapidly expanding circle

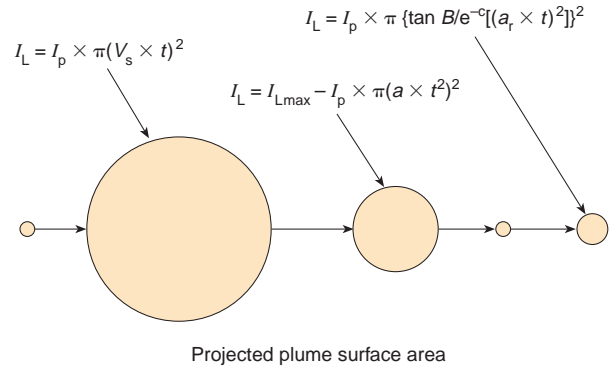


**Figure 8.** The three-stage process by which we have modeled the launch flash of a rocket booster. Stage 1 is expansion of the plume at  $V_s$  the gas expansion velocity  $\approx 330$  m/s, stage 2 is contraction at the velocity of the rocket, and stage 3 is the plume expansion with altitude (terms not defined in text are  $B$  = cone angle of booster plume,  $c$  = function of density and altitude,  $f$  = function of pressure and altitude,  $I_L$  = intensity at any plume length, and  $I_{\max}$  = intensity at maximum plume length).

with a surface irradiance  $I_p$ . Once the plume has reached its maximum expansion, it begins to collapse to  $r_{\min@sl}$  (minimum radius of the plume at surface atmospheric pressure) at a rate determined by the acceleration of the rocket  $a_r$  away from the launch pad, thereby decreasing the radius of the illuminating surface. In this model, once the plume is no longer interacting with the ground, the only light emissions come from the projected surface area of the plume. As the rocket climbs to higher altitudes, this projected area increases as a function of  $r_{\min@h}$  (radius of the plume at altitude  $h$ ) owing to reduced ambient pressure, but is bounded by the optical thickness of the emitting surface area. Results shown in Fig. 9 were generated when we applied this crude model to the data collected from each observed launch.

The results produced by this model show amplification of signal due to ground interaction and the rapid initial rise of the signal with a fall in intensity to a nearly constant level within a few seconds. These model results are comparable to observations made from space with a broadband visible sensor. Each plot in Fig. 9 is a function of booster fuel, thrust, and thrust-to-weight ratio. A more comprehensive model is likely to reproduce engine characteristics and separate fuel contributions from purely thrust factors.

## SUMMARY

The work described in this article demonstrates the viability of daytime background suppression using a narrowband optical filter centered at 589 nm and event identification from a unique intensity temporal

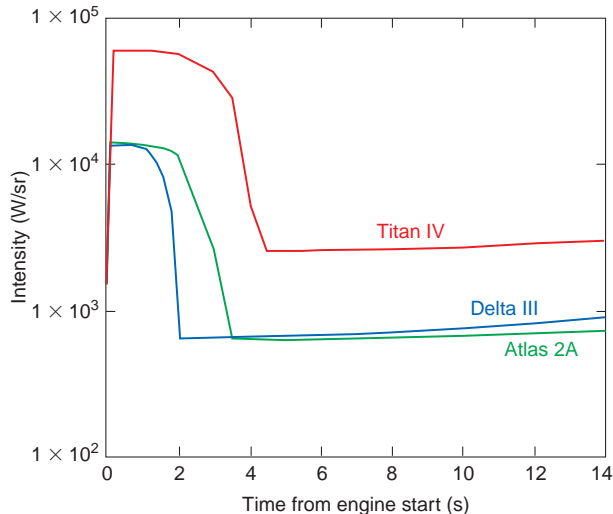


**Figure 9.** Results of expected launch temporal signatures observed from overhead obtained from a simple geometric model.

and night detection and identification of these events. This phenomenon is significant, since by using a transient event the desired information regarding the source may be gleaned within seconds of event onset, and thereby may provide an observer with the potential for rapid response.

Work to date has focused on high-speed, high-resolution imaging at narrowband visible wavelengths that simultaneously captures transient histories and suppresses background clutter from reflected sunlight. Measurements conducted at Cape Canaveral, Florida, have successfully resulted in the characterization of the ignition flash and initial plume signature from several large rocket boosters while suppressing daylight background clutter. Our initial modeling efforts are encouraging because we can reproduce the Na-line large-scale features observed from orbit in broadband. Our future work will extend to using an atomic line filter and to the development of a prototype airborne sensor platform.

**ACKNOWLEDGMENTS:** The authors wish to acknowledge the APL Independent Research and Development Sensor Thrust Area for the support of these efforts. We also wish to acknowledge the efforts of Dick Margoli and Donald Paul at APL's NOTU facility in Florida for their work in supporting our observations at Cape Canaveral.

modulation function. We have shown that the remote sensing of optical transients generated by rocket boosters at this wavelength may be practical for both day

#### THE AUTHORS



PETER F. BYTHROW joined APL's Space Department in 1981. He is a Principal Staff physicist working on the development of new space-related capabilities for the Department of Defense. Dr. Bythrow received his B.S. degree in physics from the University of Massachusetts at Lowell in 1970 (then Lowell Technological Institute). After serving as a pilot in the Air Force from 1970 to 1975, he earned his M.S. and Ph.D. degrees in space physics from the University of Texas at Dallas in 1978 and 1980, respectively. For his first 10 years at APL, Dr. Bythrow conducted research on magnetospheric plasmas and electrodynamics. He was a co-investigator on NASA and DoD space plasma and magnetic field missions, notably HILAT, Polar BEAR, and UARS. In 1988, he began work with SDIO on missile launch detection and phenomenology, and was the project scientist on the SDIO Delta 183 mission. Dr. Bythrow is currently engaged in developing new sensor technologies in surveillance, missile detection, and tracking. His e-mail address is peter.bythrow@jhuapl.edu.



DOUGLAS A. OURSLER received a B.S. in electrical engineering and computer science from The Johns Hopkins University in 1987 and an M.S. in electrical engineering from the University of Virginia. He returned to Hopkins to receive an M.S. and later a Ph.D. in materials science in 1996. As a post-doctoral fellow, he continued his research in microwave and electromagnetic techniques of nondestructive testing. Dr. Oursler co-founded a small business that developed a novel laser contouring system to map automotive body panels for the automotive and steel industries. In 1997, he joined APL's Senior Staff in the Space Department. Since then, he has been involved with the testing of the all-polymer and hybrid batteries, the development of the Xylophone Bar Magnetometer for space applications, and the investigation of optical methods for missile launch point detection. His e-mail address is douglas.oursler@jhuapl.edu.